End effects and phase instabilities in a model for Taylor-Couette systems

Daniel Walgraef
Service de Chimie-Physique II, Université Libre de Bruxelles, Campus Plaine, Code Postal 231, B-1050 Bruxelles, Belgium
(Received 10 February 1986)

The stability of Taylor vortices and the axial variation of the wavy vortex wavelength in finite Taylor-Couette geometries are studied with a model amplitude equation including nonpotential terms induced by long-wavelength inhomogeneities of the flow. The results confirm the importance of end effects in the selection and stability properties of wavy flows in agreement with various experimental results.

I. INTRODUCTION

The successive bifurcations leading to chaotic flows in Taylor-Couette experiments when the outer cylinder is at rest have been studied in great detail both theoretically and experimentally. However, the stability properties and selection mechanisms of the convective patterns remain poorly understood.[1] Moreover, it is expected that the mechanisms driving the system to its chaotic regime find their origin in the characteristics of the flow at the first instabilities. Hence there is actually a renewed interest in the study of the transitions to Taylor and wavy Taylor vortices and very careful experiments have been performed recently to study the stability regimes and the transitions between different wavy flows in different geometries.[2–5]

From the theoretical point of view, the amplitude equation formalism which led to significant progress in the study of Rayleigh-Bénard experiments, has been applied to the transition to axisymmetric Taylor vortices including fluctuations and end effects.[6,7] However, when azimuthal perturbations have to be taken into account the derivation of amplitude equations becomes more intricate[8,9] and the drift flows may play an important role even at the lowest order of the small-gap problem.[10] As the transition to wavy flows appears at higher orders of the amplitude equation expansion, a consistent derivation, even of the linear part of such equations, becomes very difficult. Indeed, owing to the radial dependence of the Couette flow, the couplings between the different components of the velocity field lead to equations of great intricacy where most of the parameters have to be estimated numerically. Furthermore, the convergence properties of the procedure are not known. Important works which are now classics in the field have been devoted to the estimation of the stability boundaries of Taylor and wavy Taylor flows along these lines but they were not able to predict the experimentally selected azimuthal wave numbers nor to incorporate satisfactorily the finite end effects in their analysis.[11,12]

This is why we recently proposed to discussed the onset of wavy flows with a model amplitude equation derived from the slow-mode dynamics of the system.[13] This formalism was already applied to other convective instabilities and to nonlinear systems with reaction-diffusion dynamics.[14–16] Other attempts devoted to theoretical descriptions of wavy flow properties have also been made by introducing phenomenological assumptions in the amplitude equation formalism[8] or by assuming the validity of a gradient expansion of the phase dynamics.[17]

However, in these approaches, crude approximations are made on the structure of the nonlinearities of the kinetic equations by neglecting nonpotential terms arising from the coupling with drift flows and from the renormalization of the wave speed. As these terms, like in other hydrodynamical systems,[18,19] may modify the stability domain of the patterns, their phase dynamics or the pattern selection in high ramping rates, one has to include them in the analysis of Taylor flows beyond their onset.

The aim of this paper is to introduce more realistic nonlinear couplings in the slow-mode dynamics, their structure being inferred from the structure of the nonlinearities of the Navier-Stokes equations, and to test the corresponding model equations on experimental observations. In Sec. II we derive and discuss the slow-mode dynamics proposed to describe the transition to axisymmetric Taylor vortices (TVF) and to wavy vortices (WVF). In Sec. III the resulting phase dynamics are obtained and their relevance to the interpretation of experimental results is discussed in Sec. IV.

II. MODEL AMPLITUDE EQUATIONS

The derivation of model amplitude equations takes advantage of the time-scale separation near the instabilities and uses the standard procedure of adiabatic elimination of the fast modes. It may be summarized as follows. Starting from the Navier-Stokes equations for the velocity fluctuations ($\mathbf{u}=u\mathbf{1}_x+v\mathbf{1}_\theta+w\mathbf{1}_z$; with x,θ,z as cylindrical coordinates) around the Couette flow [the fluid of kinematic viscosity ν is contained between two cylinders of radii ρ ($x=0$) and $\rho+d$ ($x=1$) and length L; the outer cylinder is at rest while the inner one rotates with an angular velocity Ω; the axial and radial coordinates are scaled by d, the velocity components by ν/d; the time by ν/d^2 and the pressure by $\rho\nu^2/d^2$], it is convenient to first eliminate the pressure and the axial velocity from the linear part of these equations. Then by considering that the onset of Taylor and wavy Taylor flows are very close together for small gaps, the slow modes are defined from

the projection of this linear dynamics on the eigenfunction associated to the eigenvalue vanishing at threshold, λ_1,

$$\mathbf{u}=\sum_{m,j}\int dq\,\Sigma^{(j)}_{q,m}(t)\mathbf{V}(\lambda_j,x)\exp[i(qz+m\theta)]\ , \tag{1}$$

where $\{\mathbf{V}(\lambda_j,x)\}$ is a set of orthonormalized functions determined by the linear axisymmetric problem. The slow mode is the Fourier transform $\Sigma(z,\theta,t)$ of $\Sigma^{(1)}_{q,m}(t)$. The asymptotic time evolution of its slowly varying envelope $\sigma(z,\theta,t)$

$$[\Sigma(z,\theta,t)=\sigma(z,\theta,t)\exp iq_c z+\text{c.c.}]$$

is calculated through the following small-gap decoupling:

$$\int_0^1 dx\,\mathbf{V}(\lambda_i,x)f(x)\mathbf{V}(\lambda_j,x)=f(x^*=0.5)\delta_{ij}\ . \tag{2}$$

$\mathbf{V}(\lambda_1,x)$ is determined from the eigenvalue problem,

$$\mathbf{V}(\lambda_1,x)=u(\lambda_1,x)\mathbf{1}_x+v(\lambda_1,x)\mathbf{1}_\theta+w(\lambda_1,x)\mathbf{1}_z\ ,$$

$$(DD^*-q^2-\omega)(DD^*-q^2)u-q^2\frac{2\Omega d^2}{\gamma}g(x)v=0\ ,$$

$$(DD^*-q^2-\omega)v+2\frac{\Omega d^2}{\gamma}\frac{\eta^2}{1-\eta^2}u=0\ . \tag{3}$$

The boundary conditions are $u=Du=v=0$ at $x=0,1$ and $D=(\partial/\partial x)$, $D^*=(\partial/\partial x)+(d/\rho+dx)$; $g(x)$ tends to 0.5 in the small-gap limit $\eta=(\rho/\rho+d)\to 1$. The Taylor number is defined as

$$T=2\Omega^2 d^4\eta^2/\gamma^2(1-\eta^2)$$

and ω is the growth rate of the velocity field fluctuations around the Couette flow.

By expanding the corresponding eigenvalue of the nonaxisymmetric linear evolution matrix in $(T-T_c)/T_c$, $(q^2-q_c^2)q_c^2>m^2/q_c^2\rho^2$ the linear part of the slow-mode dynamics takes the form (13)

$$\tau_0\dot{\Sigma}^{(1)}_{q,m}(t)=\left\{\frac{T-T_c}{T_c}\left[1+\frac{q^2-q_c^2}{3q_c^2}\right]+\frac{T\beta-T_c}{T_c}\frac{4m^2}{q_c^2}\left[\frac{1-\eta}{1+\eta}\right]^2-\frac{\xi_0^2}{4q_c^2}(q^2-q_c^2)^2\right.$$
$$\left.-2\xi_0^2(q^2-q_c^2)\frac{m^2}{q_c^2}\left[\frac{1-\eta}{1+\eta}\right]^2-K_0^2m^4\left[\frac{1-\eta}{1+\eta}\right]^4+im\Omega_1\left[1+2\frac{q-q_c}{q_c}\left[\frac{1-\eta}{1+\eta}\right]\right]\right\}\Sigma^{(1)}_{q,m}(t)\ , \tag{4}$$

where $\tau_0^{-1}=12.56$, $q_c=3.12$, $T_c=1708$, $\xi_0^2=0.144$,

$$\Omega_1=\Omega\eta^2(3+\eta)/(1+\eta)^3\to\Omega/2\ \text{ as }\eta\to 1$$
$$K_0^2=16\left[1+\frac{3\beta T}{T_c}\right]\Big/3q_c^4\ , \tag{5}$$
$$\beta=\frac{24}{\pi}\frac{(1+\eta)^2-2}{(1+\eta)^2(3+\eta)}\ .$$

As shown by Dominguez-Lerma *et al.*,[20] τ_0, q_c, T_c, and ξ_0 are only slightly η dependent and will be considered as constants in the following. Moreover, the wave number corresponding to the maximum growth rate of axial perturbations is found to be

$$\bar{q}=q_c\left[1+\frac{2}{3\xi_0^2q_c^2},\ \frac{T-T_c}{T_c}\right]^{1/2}\simeq q_c\left[1+0.24\frac{T-T_c}{T_c}\right] \tag{6}$$

in agreement with their calculations. The projection of the Navier-Stokes equations on $\mathbf{V}(\lambda_1,x)$ combined with the small-gap decoupling (2) eliminates the dependence on the radial coordinate thought to be irrelevant in the description of the basic characteristics of the flow. The approximations made are justified by the close vicinity of the two first thresholds (i.e., the Taylor and wavy flows) and to the particular form of the functions of the set $\{\mathbf{V}(\lambda_j,x)\}$.[21]

The linear evolution of the Fourier transform $\Sigma(z,\theta,t)$ of the slow mode is then given by

$$\tau_0\dot{\Sigma}(z,\theta,t)=\left[\frac{T-T_c}{T_c}\left[1-\frac{q_c^2+\partial_z^2}{q_c^2}\right]+\left[\frac{1-\eta}{1+\eta}\right]^2\left[\frac{T_c-\beta T}{T_c}\right]\frac{4}{q_c^2}\partial_\theta^2-\frac{\xi_0^2}{4q_c^2}(q_c^2+\partial_z^2)^2\right.$$
$$\left.-\frac{2\xi_0^2}{q_c^2}\left[\frac{1-\eta}{1+\eta}\right]^2(q_c^2+\partial_z^2)\partial_\theta^2-K_0^2\left[\frac{1-\eta}{1+\eta}\right]^4\partial_\theta^4+\Omega_1\partial_\theta\left[1-\frac{2}{q_c}\frac{1-\eta}{1+\eta}(q_c+i\partial_z)\right]\right]\Sigma(z,\theta,t)\ . \tag{7}$$

If one performs the standard multiple scale analysis on this expression one obtains the lowest-order linear part of the amplitude equation for the vortices by writing

$$\Sigma(z,\theta,t)=\sigma(z,\theta,t)\exp iq_c z+\text{c.c.}$$

The exact computation of the nonlinear terms within the framework of the amplitude equation or of the slow-mode formalism is out of the scope of our analysis as it requires a precise knowledge of the set of eigenfunctions

$\mathbf{V}(\lambda_j,x)$ and the complete adiabatic elimination of all the fast modes. However, one may guess a meaningful approximation for the nonlinearities of the slow-mode dynamics from the structure of the nonlinear couplings between the velocity components in the Navier-Stokes equations. This is sufficient for our purpose which consists in deriving a simplified version of the original Navier-Stokes equations, appropriate to describe the relevant aspects of the dynamics of the system near the first instabilities. We do not intend to obtain an approximate solution of these equations at a given order since the complexity of the calculations then often masks simple and meaningful aspects of the problem and we feel that it may be preferable to perform such expansions from a simplified model able to describe the experimentally relevant facts eventually at the lack of quantitative precision. It turns out that the nonlinear couplings between the u and w components of the velocity field lead after adiabatic elimination of the fast modes to cubic contributions to the nonlinear slow-mode dynamics. The construction of these nonlinear terms is similar to the Rayleigh-Bénard case with the difficulties encountered in the case of the realistic no-slip boundary conditions. Hence we will approximate these terms in real space by $g\,|\,\sigma\,|^2\sigma$, where g has to be determined by suitable approximations or by the fitting of experimental data[22] or numerical analysis.[6,11,23]

Other nonlinear contributions arise from the coupling between the u, v, and w components of the velocity field. These contributions come from the $w\partial_z u$ and $w\partial_z v$ of the nonlinear coupling $(\mathbf{u}\cdot\nabla)\mathbf{u}$. According to the structure of the slow-mode dynamics it turns out that these contributions lead to a term proportional to $iq_c\sigma\bar{w}_s$, where $\bar{w}$ is the slow-z varying part of w averaged over the gap

$$\bar{w}_s=\int_0^1 dx[\mathbf{V}(\lambda_1,x)]^2 w_s \simeq w_s(0.5)\ . \tag{8}$$

The evaluation of w_s requires the solution of its kinetic equation,

$$[(\partial_t-\nabla^2+\Omega\partial_\theta)w+\partial_z p+\mathbf{u}\cdot\nabla w]\,|_s=0\ . \tag{9}$$

Hence that part of the axial velocity which varies slowly in the z direction may be approximated by

$$\partial_x^2 w_s\simeq\partial_z p_s \tag{10}$$

and from the radial equation it turns out that p_s may be written as

$$p_s(x,\theta,z)=p_0(z,\theta)+h\,|\,\sigma\,|^2[\mathbf{V}(\lambda_1,x)]^2+\cdots\ , \tag{11}$$

where $p_0(z,\theta)$ is an arbitrary function which may in turn be determined by the continuity equation which requires that

$$\int_0^1 dx(\partial_z w+\partial_\theta v)=0 \tag{12}$$

leading to

$$\int_0^1 dx\,\partial_z w_s=h'\partial_\theta\,|\,\sigma\,|^2\ . \tag{13}$$

From Eqs. (10) and (11) we obtain

$$\begin{aligned} w_s(x,\theta,z)&=\partial_z p_0(z,\theta)\tfrac{1}{2}x(x-1)+h\partial_z\,|\,\sigma\,|^2\left[\int_0^x dx'-x\int_0^1 dx'\right]\int_0^{x'}dx''[\mathbf{V}(\lambda_1,x'')]^2 \\ &\simeq\partial_z p_0(z,\theta)\tfrac{1}{2}x(x-1)+\tfrac{1}{2}(x-1)h\partial_z\,|\,\sigma\,|^2\ . \end{aligned} \tag{14}$$

Moreover, from (12) we also have

$$\int_0^1 dx\frac{x(x-1)}{2}\partial_z^2 p_0(z,\theta)=-\int_0^1 dx\frac{x-1}{2}h\partial_z^2\,|\,\sigma\,|^2+h'\partial_\theta\,|\,\sigma\,|^2 \tag{15}$$

or

$$\partial_z^2 p_0(z,\theta)=-3h\partial_z^2\,|\,\sigma\,|^2-12h'\partial_\theta\,|\,\sigma\,|^2 \tag{16}$$

and finally

$$\bar{w}_s=-\tfrac{1}{8}\partial_z p_0(z,\theta)-\tfrac{1}{4}h\partial_z\,|\,\sigma\,|^2 \tag{17}$$

or

$$\partial_z\bar{w}_s=\tfrac{1}{8}h\partial_z^2\,|\,\sigma\,|^2-12h'\partial_\theta\,|\,\sigma\,|^2\ . \tag{18}$$

The approximate amplitude equation may then be written as

$$\begin{aligned} \tau_0\dot{\sigma}(z,\theta,t)=&\left\{\epsilon\left[1+\frac{2}{3iq_c}\partial_z\left[1+\frac{1}{2iq_c}\partial_z\right]\right]+\left[\frac{1-\eta}{1+\eta}\right]^2[1-(\epsilon+1)\beta]\frac{4}{q_c^2}\partial_\theta^2+\xi_0^2\left[\partial_z\left[1+\frac{1}{2iq_c}\partial_z\right]\right]^2\right. \\ &\left.+\frac{4\xi_0^2}{iq_c}\left[\frac{1-\eta}{1+\eta}\right]^2\left[\partial_z\left[1+\frac{1}{2iq_c}\partial_z\right]\right]\partial_\theta^2-K_0^2\left[\frac{1-\eta}{1+\eta}\right]^4\partial_\theta^4+\Omega_1\partial_\theta\left[1+\frac{2}{iq_c}\frac{1-\eta}{1+\eta}\partial_z\right]\right\}\sigma(z,\theta,t) \\ &-g\,|\,\sigma(z,\theta,t)\,|^2\sigma(z,\theta,t)+iq_c\sigma(z,\theta,t)\bar{w}_s\ , \end{aligned}$$

with

$$\partial_z \bar{w}_s = g' \partial_z^2 |\sigma|^2 - g'' \partial_\theta |\sigma|^2 . \quad (19)$$

In fact an eventual computation of g,g',g'' should require various integrals on elements of the set $\{\mathbf{V}(\lambda_j,x)\}$. We did not perform these calculations but from dimensional arguments it may be expected that $g' \simeq g''(1+\eta/1-\eta) \simeq g/3$.

To summarize the present discussion, let us stress the fact that we derived a system of partial differential equations governing the axial and azimuthal dependence of the local velocity field coupled to the slowly varying drift flow. These equations consist in a simplification of the original Navier-Stokes equations based on the phenomenology of the system and on the structure of the nonlinear couplings. The approximations made allow one to avoid the explicit computation of the nonlinear couplings which make the multiple scale analysis completely untractable near the transition to wavy flows. However, all the physically important qualitative features of the problem are present, and, if one performs the multiple scale analysis on this equation, the lowest-order amplitude is recovered. Let us finally point out that the approach used here was also able to improve the understanding of other convective phenomena beyond threshold.[15,24]

III. PHASE DYNAMICS AND STABILITY LIMITS OF TAYLOR AND WAVY VORTEX FLOWS

A. Phase instability of axisymmetric flows

From the kinetic equation (19) the relaxational character of the amplitude and the diffusive character of the phase of the vortices are obvious. Hence the amplitude fluctuations may be adiabatically eliminated. In the case of axisymmetric Taylor vortices, the phase dynamics may then be written at the lowest order in $\epsilon=(T-T_c)/T_c$ as

$$\tau_0 \dot{\varphi}_0 = D_0 \partial_z^2 \varphi_0 , \quad (20)$$

where

$$D_0 = \xi_0^2 \left[\frac{\epsilon - 3\xi_0^2\delta^2}{\epsilon - \xi_0^2\delta^2} - 2\frac{g' q_c}{g}\delta_0 \right]$$

and

$$\Sigma(z,\theta,t) = \sigma_0 \exp i[(q_c+\delta_0)z + \varphi_0(z,t)] + \text{c.c.}$$

For increasing values of the Reynolds number one has to take into account the deviations of $\bar{q}$ from q_c and higher contributions in ϵ to the phase dynamics. We then obtain

$$\tau_0 \dot{\bar{\varphi}} = \bar{D} \partial_z^2 \bar{\varphi} , \quad (21)$$

where

$$\bar{D} = \xi_0^2 \left[\frac{\bar{\epsilon} - 3\xi_0^2\bar{\delta}^2}{\bar{\epsilon} - \xi_0^2\bar{\delta}^2} - 2\frac{g'\bar{q}}{g}\bar{\delta} \right]$$

and

$$\bar{\epsilon} = \epsilon(1+\epsilon/g q_c^2 \xi_0^2)$$

by writing

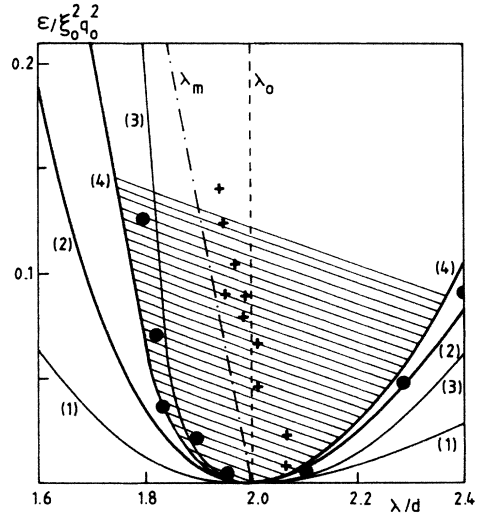

FIG. 1. Stability limits of Taylor vortex flows vs reduced wavelength $[\epsilon=(T-T_c)/T_c]$: (1) marginal stability curve, (2) Eckhaus stability limits, (3) $D_0=0$, (4) $D=0$. λ_m corresponds to the maximum growth rate, λ_0 is the critical wavelength, while the dots and crosses are the experimental results of Ahlers *et al.* (Ref. 25).

$$\Sigma(z,\theta,t) = \bar{\sigma} \exp i[(\bar{q}+\bar{\delta})z + \bar{\varphi}(z,t)] + \text{c.c.}$$

Hence the stability domain of the flow defined by $\bar{D} \geq 0$ is reduced versus the Eckhaus domain in agreement with the experimental data. The various stability limits computed for the amplitude equation and our slow dynamics are given in Fig. 1.

The experimental stability limits obtained by Ahlers *et al.*[25] are also reported on this figure (dots). Moreover as observed by these authors the wavelength selected after a sudden increase of the bifurcation parameter (crosses) is shown to be close to the maximum linear growth rate of the unstable modes which corresponds in our description to $\lambda_m = 2\pi \bar{q}_c^{-1}$ [cf. Eq. (6)], $\lambda_0 = 2\pi \bar{q}_c^{-1}$ being the critical wavelength.

B. End effects on the stability of wavy flows

In the case of a finite annulus the axial inhomogeneities of the flow induce nonvanishing contributions of the drift flow to the nonlinear terms of the kinetic equation (19) able to affect the phase dynamics. Effectively, if we let the phase fluctuate, a wavy flow of axial wavelength $2\pi q^{-1}$ and wave number m may be defined by

$$\begin{aligned}\Sigma(z,\theta,t) = {} & \sigma_0(z,t)\sin[qz+\varphi_0(z,t)] \\ & + 2\sigma_m(z,t)\cos[qz+\varphi_m(z,t)] \\ & \times \sin m(\theta-\theta_0+\Omega t) . \end{aligned} \quad (22)$$

Here also, the symmetry breaking associated with the transition to organized flows induces a time and space scale separation between phase and amplitude. The relaxational evolution of the amplitude may be adiabatically eliminated, the asymptotic evolution of the system being governed by the diffusive phase dynamics. In the case of

Eq. (19), and slightly beyond the onset of wavy flows, σ_0 is nearly homogeneous, while σ_m is modulated by end effects.[13] Moreover, the two parts of the flow remain phase locked (this is no more true for increasing values of T and may lead to further instabilities) and $\varphi_0 \simeq \varphi_m$. It turns out then that the phase dynamics may be described by the following kinetic equation:

$$\tau_0 \partial_t \varphi_0 = D_0 \partial_z^2 \varphi_0 + g' q \partial_z \sigma_m^2 \ . \tag{23}$$

σ_m was explicitly calculated for $q = q_c$ in Ref. 13. A similar calculation may be performed for $q \neq q_c$ since by inserting the expression for the flow given by Eq. (22) into the kinetic equation (19), the stationary amplitude of the azimuthal part of the flow, σ_m, is given by

$$\left[\frac{4m^2\beta}{q_c^2} \left(\frac{1-\eta}{1+\eta} \right)^2 \frac{T - T_w(m,q)}{T_c} + \xi_0^2 \partial_z^2 \right] \sigma_m(z) - 2g\sigma_m^3(z) = 0 \ , \tag{24a}$$

where

$$T_w(m,q) = T_c \beta^{-1} \left[1 + \frac{16m^2}{q_c^2} \left(\frac{1-\eta}{1+\eta} \right)^2 + \frac{3\xi_0^2}{4q_c^2} (q^2 - q_c^2)^2 \right] . \tag{24b}$$

As σ_m has to vanish at the cylinders ends [$\sigma_m(0) = \sigma_m(L) = 0$], it may be written as

$$\sigma_m(z) = \bar{\sigma}_m \sin \phi_m(z) \ , \tag{25a}$$

with

$$z = \left[\frac{\xi_0^2(1+k^2)}{\epsilon_m} \right]^{1/2} \int_0^{\phi} d\alpha (1 - k^2 \sin^2 \alpha)^{-1/2} \ , \tag{25b}$$

where

$$\bar{\sigma}_m^2 = 2\epsilon_m k^2 / (1+k^2) g \tag{25c}$$

and

$$L = 2 \left[\frac{\xi_0^2(1+k^2)}{\epsilon_m} \right]^{1/2} K(k) \ ,$$
$$\epsilon_m = \frac{4m^2\beta}{q_c^2} \left(\frac{1-\eta}{1+\eta} \right)^2 \frac{T - T_w(m,q)}{T_c} \ . \tag{25d}$$

Since this solution only exists for

$$L \geq L_c = d\pi (\xi_0^2/\epsilon_m)^{1/2}$$

or

$$\epsilon_m \geq \xi_0^2 (\pi d/L)^2 \ ,$$

the corresponding threshold is defined by

$$T = T_W(m,q;L) = T_c \beta^{-1} \left[1 + \frac{16m^2}{q_c^2} \left(\frac{1-\eta}{1+\eta} \right)^2 + \frac{3\xi_0^2}{4q_c^2} (q^2 - q_c^2)^2 + \frac{q_c^2 \xi_0^2}{4m^2} \left(\frac{1+\eta}{1-\eta} \right)^2 \left(\frac{\pi d}{L} \right)^2 \right] . \tag{26}$$

Slightly beyond this threshold, the small-k limit may be taken in Eq. (25) and one has

$$k^2 = 1 - \frac{\xi_0^2}{\epsilon_m} \left(\frac{\pi d}{L} \right)^2 ,$$
$$\phi_m = \left(\frac{\epsilon_m}{\xi_0^2} \right)^{1/2} z = \frac{2K(0)}{L} z = \frac{\pi z}{L} \ , \tag{27a}$$

and

$$\bar{\sigma}_m^2 = 2 \left[\epsilon_m - \xi_0^2 \left(\frac{\pi d}{L} \right)^2 \right] / g \tag{27b}$$

leading to

$$\sigma_m(z) = \left[\frac{8m^2\beta}{q_c^2} \left(\frac{1-\eta}{1+\eta} \right)^2 \frac{T - T_W(m,q;L)}{gT_c} \right]^{1/2} \sin \frac{\pi z}{L} \ . \tag{27c}$$

By increasing the Reynolds number, ϵ_m and consequently k increases, leading to a more angular shape for σ_m, whose maximum tends to ϵ_m / g.

Since the flow has to fit into the annulus, it turns out that the local axial wavelength, deduced from Eqs. (23) and (18) of Ref. 13 may be written as

$$\lambda = \frac{L}{N} \left[1 + \frac{g' \sigma_m^2}{D_0} \left(\frac{1}{L} \int_0^L dz' \sin^2 \phi_m(z') - \sin^2 \phi_m(z) \right) \right]^{-1} \tag{28}$$

or, near threshold,

$$\lambda = \frac{L}{N} \left\{ 1 + \frac{4g' m^2 \beta}{g \xi_0^2} \left(\frac{1-\eta}{1+\eta} \right)^2 \frac{T - T_W}{T_c} \times \left[1 - 2 \sin^2 \left(\frac{\pi z}{L} \right) \right] \right\}^{-1} \tag{29}$$

(N being the number of vortex pairs in the column).

The corresponding variation of the wavelength along the annulus for increasing values of the Taylor number may be visualized in Fig. 2. One sees that the vortices are

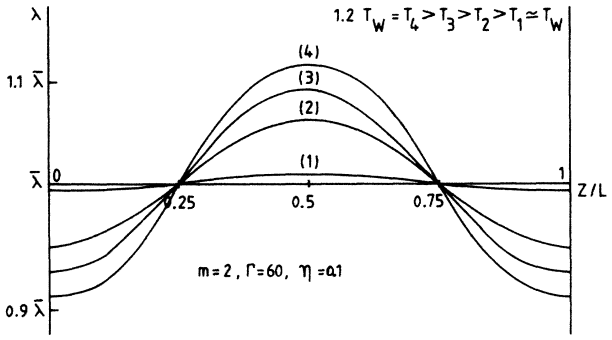

FIG. 2. Variation of the local wavelength of wavy vortices vs their axial position for different Taylor numbers [the units are arbitrary but it should be noted that, by using Eq. (29) and the numerical values of λ_0, ξ_0^2, T_W deduced from Eqs. (4) and (26) one obtains, for $\eta = 0.9$ and $m = 2,3$ a variation of the wavelength within the range of experimental data (Refs. 2 and 5)].

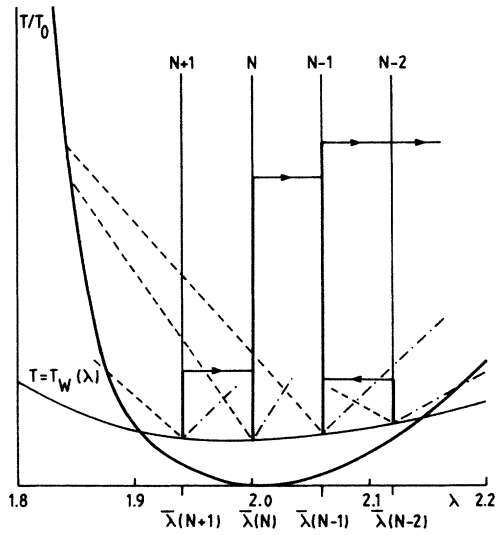

FIG. 3. Transition mechanism between wavy vortex flows with different number of vortex pairs: the dashed lines are the minimum local wavelengths; the dash-dotted lines are the maximum wavelengths; $\bar{\lambda}(N)$ is the mean wavelength of a flow with N vortex pairs.

compressed at the ends and expanded at the center of the cylinder in agreement with different experiments.[2,5] When the local wavelength reaches the stability boundaries, a transition occurs by the suppression or addition of a vortex pair in a way which is very similar to the experimental observations.[2–5] This transition mechanism is schematically illustrated in Fig. 3.

IV. DISCUSSION

The transitions between wavy flows with different number of vortex pairs and due to the mechanism discussed in Sec. III were computed for realistic values of the parameters. The results, displayed in Figs. 4 to 6 show a reasonable agreement with the corresponding experimental data.[2,5]

We effectively see that the stability domain of wavy vortex flows is considerably reduced and takes a nearly triangular shape. The following behavior of the system is expected for slow increases of the Reynolds number beyond the WVF threshold: the axial wavelength of the flow loses its uniformity and the vortices are expanded at the center of the column and compressed near the ends; when the local wavelength reaches the phase instability boundary ($D_0=D_{||}=0$) the flow should reorganize itself by losing or gaining a vortex pair; successive transitions of this type will occur till the flow reaches a point where a reorganization of this type is not possible anymore within the stability limits of the flow.

In this case it has to modify its azimuthal wave number as well. But, if there is no overlapping between the respective stability domains (cf. also Fig. 8), the flow is expected to become ill defined, including defect activity and temporal behavior before reaching a new organized pattern with a different m at a higher value of the Reynolds number.

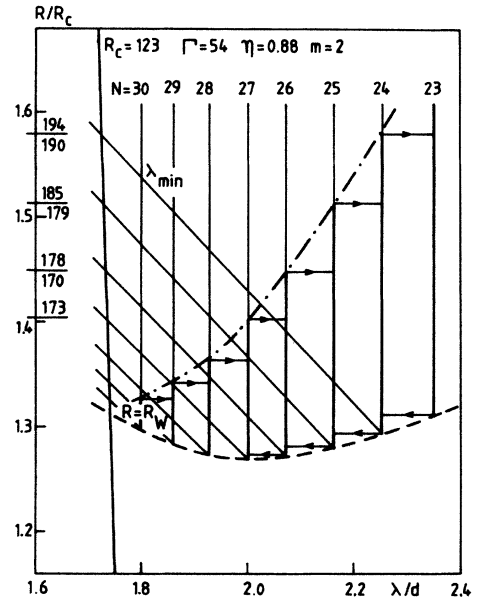

FIG. 4. Transitions between wavy vortex flows with different number of vortex pairs for values of the parameters corresponding to the experiments of the Oregon group (Refs. 3 and 5). The Reynolds numbers corresponding to the transitions are indicated on the left of the figure (above the transition line: theoretical value, below the transition line: experimental value).

The curves presented in the figures were obtained with the values of the parameters $\tau_0, q_c, \xi_0, K_0, \beta$ given in Eq. (5), η and Γ corresponding to experimental values. In the computation of the stability limits, the nonlinear coupling constants only appear via the ratio g'/g which was assumed to be of the order of one-third as a result of scaling properties. As this ratio affects the variation of $\lambda_{\min}$ and $\lambda_{\max}$ with R/R_c, its value defines the shape and area of the stability domain of wavy flows but does not affect the

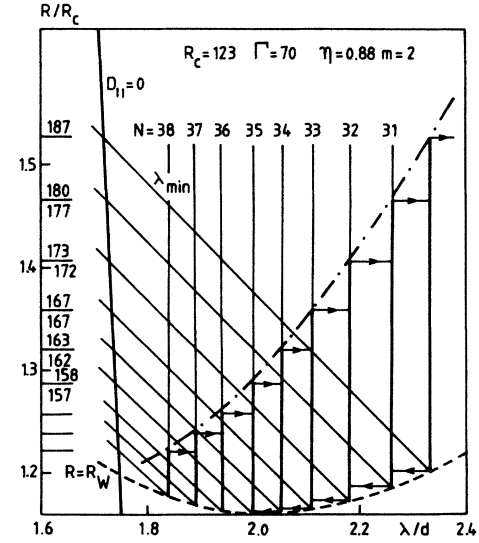

FIG. 5. Transitions between different wavy flows as in Fig. 4 but for a higher value of the aspect ratio.

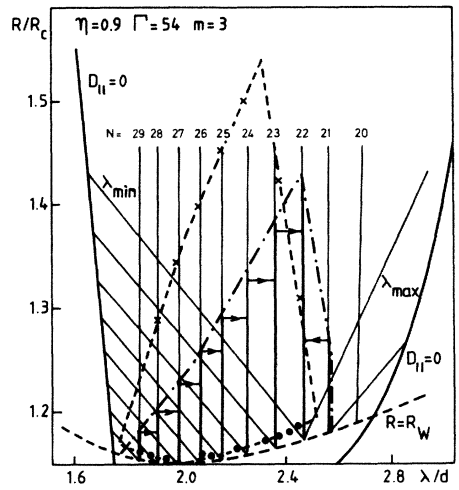

FIG. 6. Transitions between wavy vortex flows with different number of vortex pairs for values of the parameters corresponding to the experiments of the Santa Barbara group. Dots and crosses correspond to experimental results (Ref. 2).

origin nor the mechanism of the deterministic transition between wavy flows with different numbers of vortex pairs.

More recently, Bust, Dornblaser, and Koschmieder[26] studied the amplitudes and wavelengths of wavy vortices in water and 10-cs silicone oil. Their apparatus having a radius ratio of 0.885 and an aspect ratio of 31.02, the first wavy vortex state to appear after a slow increase of the Reynolds number is expected to be a state with 15 vortex pairs and an azimuthal wave number 4,[13] the threshold being $R=1.19R_c$. This seems to be the experimental situation. Moreover, the increase of the wave height and of the wavelength at the center of the column is in qualitative agreement with the present theoretical analysis. Values of the wave heights obtained from our model are given in Fig. 7. They are very sensitive to the parameters

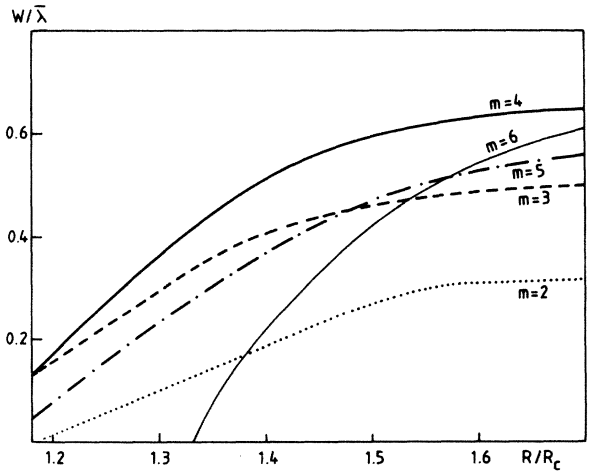

FIG. 7. Reduced wave heights vs Reynolds number for different values of the azimuthal wave number ($\eta=0.885$, $\Gamma=31.02$).

of the problem and this may explain the relatively scattered experimental data.

For example, a variation of η from 0.88 to 0.9 for $\Gamma=30$ leads to a 10% shift of the threshold of wavy flows with azimuthal wave number 2, and a 40% decrease of the corresponding wave height at saturation ($T\gg T_c$). Furthermore the viscosity dependence of the experimental observations is not reflected in our model as the viscosity dependence of the linear terms has been incorporated in the Reynolds number. A viscosity dependence should nevertheless appear in nonlinear couplings but as we took g as a constant, it does not appear in the maximum wave height which is proportional to

$$\sigma_m(L/2)/\sigma(0)=8m^2\beta q_c^{-2}[(1-\eta)/(1+\eta)]^2 \times[T-T_W(m,q;L)]/(T-T_c)\ .$$

In fact, for increasing values of the Taylor number, as already mentioned in Ref. 13, the nonlinear couplings involving axial or azimuthal flows should be slightly different leading to a viscosity dependence of the wave height. However, this dependence, appearing through terms proportional to $m^2q_c^{-2}\rho^{-2}$, is not expected to be as important as the experimentally observed one.

It is now clear from the above discussion that the slow-mode dynamical concepts used here, by avoiding the complexity and inconsistencies of the higher-order amplitude equations, are able to give some insights on the pattern-selection mechanisms for Taylor and wavy vortex flows as well as on transition mechanisms between simultaneously stable flows.

As in other problems where transitions occur via the spontaneous breaking of continuous symmetries, one expects, in the wavy mode regime also, the nucleation of long-range phase fluctuations inducing dislocationlike defects in the flow. According to the stochastic analysis of this phenemenon, the probability associated to such defects, should be maximum near the stability boundaries, where the phase diffusion coefficient vanishes. As a high defect probability may lead to the complete deorganization of the structure and to spatial chaos, this could explain the presence of chaotic regions between different wavy flow regimes as observed by Donnelly *et al.*[27] and confirmed by King and Swinney.[4] This is illustrated in Fig. 8. This figure shows the stability domains of wavy flows with different azimuthal wave numbers and computed from Eq. (28) for $\eta=0.875$ and $\Gamma=80$. It has to be noted that near onset the whole flow is affected by the end effects and the approximation (29) is valid. However, for increasing ϵ_m, i.e., for increasing R or m, the z-dependent wavelength is no more sinusoidal but has a kink shape. In this case the wavelength is nearly constant over most of the annulus height and is rapidly decreasing near the ends. When the corresponding healing length becomes less than a mean wavelength, we may consider that the flow remains stable. This defines the curves $R_w'(m)$ and leads to the peculiar shape of the stability domain for $m=6$ which is reminiscent of the results of King and Swinney.[4] Furthermore this argument justifies the possibility of a reappearance of flows with low m at higher values of the Reynolds number. For example, flows with 40 vortex

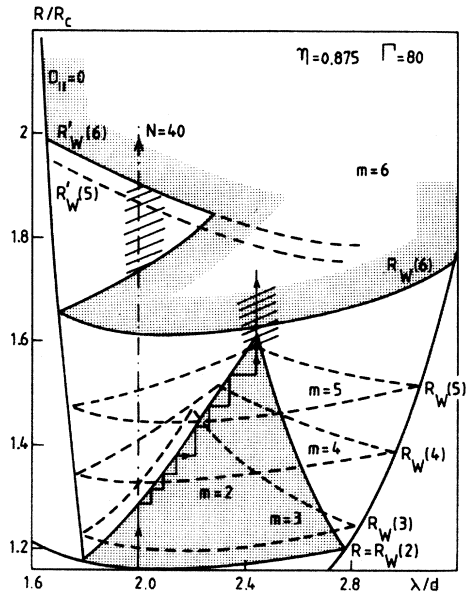

FIG. 8. Stability diagram and transitions between different wavy flows for realistic values of the radius and aspect ratios. $R_W(m)$ are the loci of critical Reynolds numbers associated to wavy flows of azimuthal wave number m [cf. Eq. (25)]. $R'_W(m)$ is defined in the text. The dashed lines are stability boundaries while the dotted regions are the stability domains of $m=2$ and $m=6$ flows. Plain arrows represents the theoretical succession of patterns in a quasistatic experiment while the dash-dotted arrow represent sudden increases of the bifurcation parameter. Hatched regions on these arrows correspond to high defect activity associated to low values of the phase diffusion coefficients.

pairs and $m=5$ may reappear at $R=1.86R_c$, $m=4$ at $R=2.05R_c$, $m=3$ at $R=2.4R_c$, and $m=2$ at $R=3.9R_c$.

Hence if one starts an experiment with a quasistatic increase of the Reynolds number, the present model predicts, for $\eta=0.875$ and $\Gamma=80$, the appearance, at $R/R_c=1.16$, of a flow with $N=40$ vortex pairs and $m=2$.

The stability domain of the $m=2$ flow is the lowest dotted region of the diagram. By increasing R beyond $1.16R_c$, successive transitions then occur as in the previously discussed experiments, leading to a decrease in the number of vortex pairs down to 33. Beyond this point no further variation in the vortex number is possible and any $m=2$ flow becomes unstable. The next transition leads then to a $m=6$ flow. Between these two states an intense dislocation activity is expected due to the proximity of the stability limits (hatched regions of the phase diagram) and to the absence of overlapping between the respective stability domains. A rapid increase of R, on the contrary, may lead to an arbitrary succession of flows with increasing m. Moreover, beyond $R_W(6)$, we see that on the $\lambda=2d$ line, for example, a region exists between two $m=6$ regimes where any wavy flow is unstable. In the case of a rapid increase of R and with an initial flow including 40 vortex pairs one should then observe the following flow sequence: $(N=40,m=6)\rightarrow$chaotic regime $\rightarrow(N=40,m=6)$.

To conclude, let us emphasize that the various examples discussed here show the importance of local drift flows on the stability of the Taylor and wavy Taylor vortices in the presence of slight axial inhomogeneities. The simple form used to describe these flows in our model is able to reproduce at least qualitatively many experimental observations. As a consequence, all the stability properties of wavy flows, which have inevitably axially inhomogeneous envelopes due to end effects, are expected to be extremely sensitive to these nonpotential drift terms which need to be included in any further study of pattern selection in Taylor-Couette experiments.

However, in order to be able to describe the next instabilities by lifting, for example, the locking approximation for the phases of the axial and azimuthal parts of the flow, a more precise knowledge of the nonlinear coupling constants is required as a better insight of the validity range of the approximation made so far. Effectively, the validity of the model is expected to depend on the distance $\epsilon=(T-T_c)/T_c$ to the instability of the Couette flow and on the smallness of the gap between the two cylinders. But, as the convergence radius of the multiple scale expansion performed to obtain Eq. (4) is not known this dependence is difficult to assess. Hence the situation should be similar here to what happens in the study of Rayleigh-Bénard convection where various models have been studied numerically and analytically and tested experimentally. For example, experimental results were shown to be consistent with the Swift-Hohenberg model up to a distance $\epsilon\simeq 2$ above the onset of convection.[28] Furthermore, in the present case, the predictions of the lowest-order amplitude equation agree with the experimental study of the onset of Taylor vortices.[29] As the model discussed here is a natural extension of it and is already able to qualitatively reproduce various experimental observations, we suggest that it could be useful for a quantitative study of the selection and stability properties of wavy flows in different geometries, including the effect of nonpotential drift terms.

ACKNOWLEDGMENTS

I am grateful to G. Ahlers, P. Borckmans, G. Dewel, R. J. Donnelly, and K. Park for helpful discussions. I acknowledge support from Fonds National de la Recherche Scientifique de Belgique.

[1]R. C. Di Prima and H. L. Swinney, in *Hydrodynamic Instabilities and the Transition to Turbulence,* edited by H. L. Swinney and J. P. Gollub (Springer, Berlin, 1981), Chap. 6.

[2]G. Ahlers, D. S. Cannell, and M. A. Dominguez-Lerma, Phys. Rev. Lett. **49**, 368 (1982); Phys. Rev. A **27**, 1225 (1983).

[3]K. Park and G. L. Crawford, Phys. Rev. Lett. **50**, 343 (1983).

[4]G. P. King and H. L. Swinney, Phys. Rev. A **27**, 1240 (1983).

[5]K. Park, G. L. Crawford, and R. J. Donnelly, Phys. Rev. Lett.

51, 1352 (1983).
[6]R. Graham and J. A. Domaradski, Phys. Rev. A **26**, 1572 (1982).
[7]D. Walgraef, P. Borckmans, and G. Dewel, Phys. Rev. A **25**, 2860 (1982).
[8]H. Brand and M. C. Cross, Phys. Rev. A **27**, 1237 (1983).
[9]P. Tabeling, J. Phys. (Paris) Lett. **44**, L-665 (1983).
[10]P. Hall, Phys. Rev. A **29**, 2921 (1984).
[11]A. Davey, R. C. Di Prima, and J. T. Stuart, J. Fluid. Mech. **31**, 17 (1968).
[12]R. Krueger, A. Gross, and R. C. Di Prima, J. Fluid. Mech. **24**, 521 (1966).
[13]D. Walgraef, P. Borckmans, and G. Dewel, Phys. Rev. A **29**, 1514 (1984).
[14]J. Swift and P. C. Hohenberg, Phys. Rev. A **15**, 319 (1977).
[15]P. Manneville, J. Phys. (Paris) **44**, 759 (1983).
[16]D. Walgraef, P. Borckmans, and G. Dewel, Adv. Chem. Phys. **49**, 311 (1982).
[17]H. R. Brand, Prog. Theor. Phys. **71**, 1096 (1984).
[18]H. S. Greenside and M. C. Cross, Phys. Rev. A **31**, 2492 (1985).
[19]D. Walgraef, P. Borckmans, and G. Dewel, Springer Proc. Phys. **1**, 50 (1984).
[20]M. A. Dominguez-Lerma, G. Ahlers, and D. S. Cannell, Phys. Fluids **27**, 856 (1984).
[21]S. Chandrasekhar, *Hydrodynamics and Hydrodynamic Stability* (Clarendon, Oxford, 1961).
[22]J. P. Gollub and M. H. Freilich, Phys. Fluids **19**, 619 (1976).
[23]H. Yahata, Prog. Theor. Phys. **57**, 1490 (1977).
[24]J. E. Wesfreid and S. Zaleski, *Cellular Structures and Instabilities,* Vol. 210 of *Lecture Notes in Physics* (Springer, Berlin, 1984).
[25]G. Ahlers and D. S. Cannell, Phys. Rev. Lett. **50**, 1365 (1983); **50**, 1583 (1983).
[26]G. S. Burst, B. C. Dornblaser, and E. L. Koschmieder, Phys. Fluids **28**, 1243 (1985).
[27]R. J. Donnelly, K. Park, R. Shaw, and R. W. Walden, Phys. Rev. Lett. **44**, 987 (1980).
[28]M. S. Heutmaker, P. N. Fraenkel, and J. P. Gollub, Phys. Rev. Lett. **54**, 1369 (1985).
[29]R. Heinrichs, G. Ahlers, and D. S. Cannell, Phys. Rev. Lett. **56**, 1794 (1986).

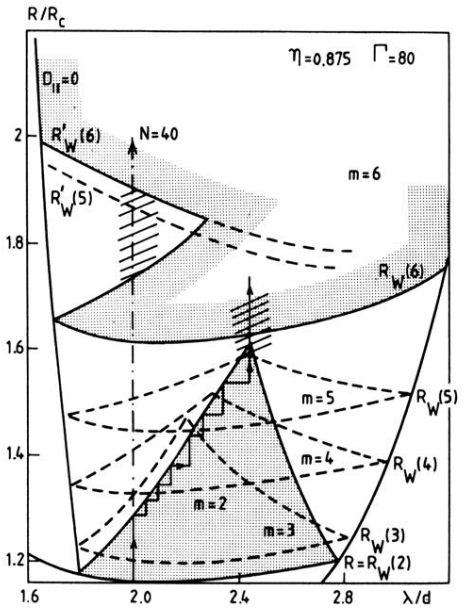

FIG. 8. Stability diagram and transitions between different wavy flows for realistic values of the radius and aspect ratios. $R_W(m)$ are the loci of critical Reynolds numbers associated to wavy flows of azimuthal wave number m [cf. Eq. (25)]. $R'_W(m)$ is defined in the text. The dashed lines are stability boundaries while the dotted regions are the stability domains of $m=2$ and $m=6$ flows. Plain arrows represents the theoretical succession of patterns in a quasistatic experiment while the dash-dotted arrow represent sudden increases of the bifurcation parameter. Hatched regions on these arrows correspond to high defect activity associated to low values of the phase diffusion coefficients.